Journal of Power Sources 227 (2013) 243–253

Contents lists available at SciVerse ScienceDirect

Journal of Power Sources

journal homepage: www.elsevier.com/locate/jpowsour

Modelling the micro–macro homogeneous cycling behaviour of a lithium–air battery

Ukrit Sahapatsombut*, Hua Cheng, Keith Scott

School of Chemical Engineering and Advanced Materials, Newcastle University, Merz Court, Newcastle upon Tyne NE1 7RU, UK

HIGHLIGHTS

- A micro–macro homogeneous model is developed for a rechargeable Li–air battery.
- The model includes the mass transport through the lithium oxide layer.
- The model can simulate the discharge and charge feature without parasitic reactions.
- Effects of cathode structure and feeding conditions have been investigated.

ARTICLE INFO

Article history:
Received 31 August 2012
Received in revised form
24 October 2012
Accepted 16 November 2012
Available online 23 November 2012

Keywords:
Li–air battery
Macro-homogeneous model
Porous cathode
Discharge capacity
Charge/discharge cycle

ABSTRACT

A micro–macro homogeneous mathematical model is developed for a rechargeable Li–air battery using a concentrated binary electrolyte theory. The dynamic behaviour of the porous cathode is determined by a numerical solution of the combined continuity, transport and kinetics equations. This model considers the time and space dependence of the battery system, including the mass transport along the depth of the cell, the local mass transfer between lithium peroxide (Li_2O_2) layer inside the cathode and active surface morphology changing with the Li_2O_2 growth. The model predicts that the battery capacity and discharge potential are sensitive not only to the solubility of oxygen, which is predominantly limited by depletion of the oxygen concentration, as well as to the cathode porosity, the cathode structure and kinetic parameters. In addition, the charging behaviour is simulated by modelling the dissolution of solid Li_2O_2 product. The model suggests that the charging voltage can be lowered depending on capability of electrolyte to dissolve the Li_2O_2 discharge products. As a result, a simulation of electrode behaviour is obtained.

1. Introduction

The development of high performance and light weight energy storage devices has recently focused on the rechargeable lithium–air batteries. Mainly due to their high energy density, theoretically up to 11,400 Wh kg^{-1} (which is about 10 times greater than well-known lithium-ion battery), such batteries are now considered as one of the promising alternatives to lithium-ion batteries with potentially wide applications, from small portable electronics to electric vehicles. The first Li–air system with a non-aqueous electrolyte was presented by Abraham and Jiang in 1996 [1]. After their promising rechargeable ability was demonstrated by Bruce group [2], Li–air batteries have attracted much more attention [2–7].

As shown in Fig. 1, a Li–air battery contains a metal lithium anode, a solid polymer separator and a porous carbon or catalyst-loaded carbon air electrode filled with an organic electrolyte comprising a dissolve lithium salt in an aprotic solvent. The porous carbon electrode provides a site for electrochemical reduction of oxygen and, during battery operation, oxygen (comes from the external air) is dissolved in the electrolyte, penetrates through the pore of the cathode and reacts with the lithium ion (Li^+) at the active site. It is important to understand the oxygen reduction mechanisms, including intermediate steps (e.g. discharge products formation). Up to date, there are various mechanisms for oxygen reduction reaction (ORR), related to type of electrolyte, catalyst and battery operating conditions. Peng et al. [8] investigated in situ spectroscopic data of oxygen reaction in a non-aqueous electrolyte and found strong evidence that lithium superoxide (LiO_2) is indeed an intermediate species during oxygen reduction before disproportion to final Li_2O_2 product. For battery charging, the reaction is simply the oxidation of Li_2O_2 directly into oxygen and Li^+ without

* Corresponding author. Tel.: +44 191 222 5207; fax: +44 191 222 5292.
E-mail address: ukrit.sahapatsombut@ncl.ac.uk (U. Sahapatsombut).

0378-7753/$ – see front matter © 2012 Elsevier B.V. All rights reserved.
http://dx.doi.org/10.1016/j.jpowsour.2012.11.053

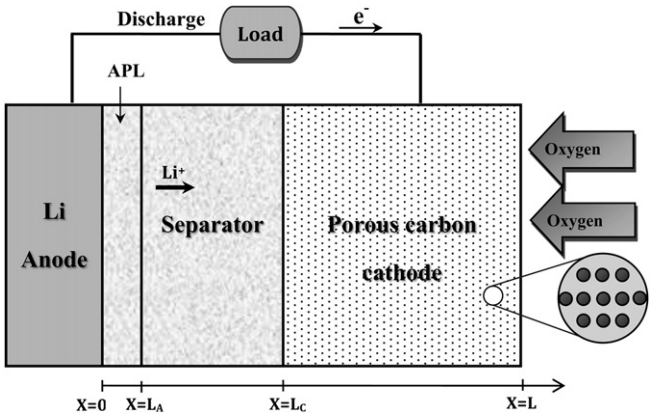

Fig. 1. Schematic diagram computation domain of a Li–air cell during discharge. The inset demonstrates the porous carbon cathode.

passing intermediate LiO_2 route. Based on literature [1,9,10], our model assumes the following battery reactions:

Anode

$$Li \rightarrow Li^+ + e^- \quad (E^0 = 0.00\ V) \tag{I}$$

Cathode

$$2Li^+ + O_2 + 2e^- \rightarrow Li_2O_2 \quad (E^0 = 2.96\ V) \tag{II}$$

$$4Li^+ + O_2 + 4e^- \rightarrow 2Li_2O \quad (E^0 = 2.91\ V) \tag{III}$$

Li_2O_2 is the main reaction product considered in this model because it is insoluble in the organic electrolyte and could cover on the active surface area inside the porous cathode as well as block the pathway for reactive species (Li^+ and oxygen), preventing further reactions inside the cathode and contributing to the end of cell discharge [9,10]. Conversion of Li_2O_2 to Li_2O is not considered because, if any, it only occurs at a significant more negative (lower) potential below 2 V, which is beyond the potential range of the model. Thus, a micro–macro homogeneous mathematical model, dealing with the entire electrode–electrolyte cell system as two continua (one from the electrode matrix and the other from the solution filling in all the space of the electrode), is developed for the cycling operation of a porous cathode of a rechargeable Li–air battery using a concentrated binary electrolyte theory [11,12]. The model predicts the time dependence of electrolyte concentration, non-uniform porosity and reaction rate. The more accurate kinetic reaction in a porous cathode is established by including the dependency of the diffusion transport on reactant concentrations and the solubility limit of the product. The model also includes the mass transport along the depth of the cell, the local mass transfer between Li_2O_2 layers and active surface morphology changing with the Li_2O_2 formation. Important parameters, such as porosity and thickness of electrode, electrolyte transport properties and surface activity, are investigated through this modelling study. The model predicts the direction of improving the Li–air battery performance in term of the discharge product formation and dynamic model parameters.

Different from previous approaches [13,14], assuming that the cathode only contains a large number of cylindrical pores without considering the macroscopic aspects, our model considers electrochemical kinetic dependency on both Li^+ and oxygen species and includes local mass transport through the solid Li_2O_2 layer. In addition, variable physical and chemical properties are carefully applied in the model based on available published experiment data. Therefore, this model can be used to describe the behaviour of Li–air batteries as well as to optimise the performance of these batteries.

2. Model development

2.1. Basic equations

A mathematical description for a prismatic of Li–air battery has been developed involving conservation of mass and current, species transport, and reaction kinetic in the cathode and separator to clarify the mechanism inside the cell. The model used in this work is for a Li–air cell consisting of a thin lithium sheet negative electrode, an anode protective layer (APL), a separator, and a porous carbon oxygen/air cathode filled with an organic electrolyte as shown in Fig. 1. Current collectors are placed at the back of each electrode. A concentrated binary electrolyte theory is used to describe the motion for of each species in the electrolytic solution. The Li_2O_2 formation inside the porous cathode is presented using macro-homogeneous porous model, defining the electrode by its porosity which is initially uniform but changes during discharge. The macroscopic theory of porous electrode treats the solution and solid matrix phases as superimposed continuum. Based on this approach, a material balance equation for specie i in the electrolyte solution phase can be expressed as

$$\frac{\partial(\varepsilon c_i)}{\partial t} = -\nabla \cdot \boldsymbol{N}_i + r_i \tag{1}$$

where c_i is the bulk concentration of species i in the solution phase which is averaged over the volume of the solution in the pores, ε is the porosity of the electrode which is the electrolyte space in the solution phase, $\boldsymbol{N}_i$ is the molar flux of species i in the porous solution averaged over the cross sectional area of the electrode, and r_i is the volumetric production rate of species i from the solid phase (electrode material) to solution phase (electrolyte in the porous) within the porous electrode. The concentration of lithium electrolyte is the same as concentration of Li^+ due to the binary electrolyte assumption. Without convection term, the diffusion and migration fluxes equations for mass transfers for both Li^+ and oxygen in the cell can be expressed as

$$\boldsymbol{N_{Li}} = -D_{Li,eff}\nabla c_{Li} + \frac{\boldsymbol{i}_2 t_+}{F} \tag{2}$$

$$\boldsymbol{N_{O_2}} = -D_{O_2,eff}\nabla c_{O_2} \tag{3}$$

where $D_{Li,eff}$ and $D_{O_2,eff}$ are the effective diffusion coefficient of Li^+ and O_2, respectively, t_+ is the transference number of Li^+, F is Faraday's constant which is equal to 96,485 C mol^{-1}, and $\boldsymbol{i}_2$ is the current density in the solution phase or electrolyte current density which can be defined by the gradient of the potential in concentrated electrolyte solution as [15,16]

$$\nabla\phi_2 = -\frac{\boldsymbol{i}_2}{\kappa_{eff}} - \frac{\nu RT}{F}\left(\frac{s_+}{n\nu_+} + \frac{t_+}{z_+\nu_+} - \frac{s_0 c}{nc_0}\right)\left(1 + \frac{\partial lnf}{\partial lnc}\right)\nabla lnc \tag{4}$$

where n, s_+, s_0, ν_+, and ν represent the number of electrons transferred, the stoichiometric coefficients for cation and solvent, the numbers of cation, and the number of moles of ions into which a mole of electrolyte dissociates, respectively. c and c_0 are the molar concentrations of the electrolyte and solvent in the electrolyte

phase, respectively. In Li–air battery, a 1:1 binary electrolyte is applied in the cell. Then, $s_0 = 0$, $s_+ = -1$, $\nu_+ = n = 1$, and $\nu = 2$. The Eq. (4) can be rearranged into the current density in electrolyte as

$$\boldsymbol{i}_2 = -\kappa_{eff}\nabla\phi_2 - \frac{2RT\kappa_{eff}}{F}(t_+ - 1)\left(1 + \frac{\partial lnf}{\partial lnc_{Li}}\right)\nabla lnc_{Li} \quad (5)$$

where κ_{eff} is the effective conductivity of the electrolyte, ϕ_2 is the electrolyte potential (electric potential of Li^+), R is the universal gas constant which is equal to 8.3143 J mol^{-1} K^{-1}, T is the cell temperature in Kelvin, and f is the activity coefficient of $LiPF_6$ salt.

In the solid matrix phase, the movement of electron is governed by Ohm's law which computes the electric potential or potential of electron, ϕ_1

$$\boldsymbol{i}_1 = -\sigma_{eff}\nabla\phi_1 \quad (6)$$

where σ_{eff} is the effective conductivity of the electron in the electrode. This parameter is affected by the volume fraction of solid electrode. The effective parameters D_{eff}, κ_{eff} and σ_{eff} in the above equations are usually depend on the tortuosity of individual phase in porous cathode (through porosity or volume fraction). These parameters are applied for only the porous cathode region (others are not porosity) and are corrected to account for the porosity effect using Bruggeman correlation [17]

$$D_{Li,eff} = \varepsilon^{1.5}D_{Li} \quad (7)$$

$$D_{O_2,eff} = \varepsilon^{1.5}D_{O_2} \quad (8)$$

$$\kappa_{eff} = \varepsilon^{1.5}\kappa \quad (9)$$

$$\sigma_{eff} = (1-\varepsilon)^{1.5}\sigma \quad (10)$$

where D_{Li}, D_{O_2}, κ and σ are the diffusion coefficient of the Li^+ and O_2 in electrolyte and the conductivity of electrolyte and electron in the cathode, respectively

2.2. Conservation of charge

For the macroscopic model, the charge conservation between the solid phase and solution phase is zero and can be expressed as the divergence of the total current density defined by

$$\nabla\cdot\boldsymbol{i}_1 + \nabla\cdot\boldsymbol{i}_2 = 0 \quad (11)$$

During discharge or charge, the oxidation and reductions occurring at the electrode/electrolyte interface (charges transfer reaction) at individual electrode are represented in the general formula in Eq. (12). The charge transfer from solid phase to electrolyte phase per unit volume of electrode ($\nabla\cdot\boldsymbol{i}_2$) is related to the average transfer current density given in Eq. (13).

$$\sum s_i M_i^{z_i} \rightarrow ne^- \quad (12)$$

$$\nabla\cdot\boldsymbol{i}_2 = aj \quad (13)$$

This equation states that the transfer current per unit electrode volume is equivalent to the electrode chemical reaction rate where the M_i is a species symbol participating in the electrochemical reaction, z_i and s_i are the charge number and the stoichiometric coefficient of the species i, n is the number of electron transferred in the reaction, a is the specific interfacial area of the pore per unit volume of the total electrode, and j is the average transfer current density. The value of s_i, z_i, and n can be defined by matching with an individual electrode reaction using general form of Eq. (12), for example, the value of s_{Li}, z_{Li}, and n of Li^+ from Eq. II are −2, 1, and 2, respectively.

Only one electrochemical reaction, i.e. Li_2O_2 formation inside porous electrode, is considered in the present work. In practical cell, the battery side reactions during cycling can occur along with the main electrode reactions. This is reflected by the superficial production rate of a species from solid phase to pore solution, given by Faraday's law

$$r_i = -\frac{as_i}{nF}j_c \quad (14)$$

2.3. Rate expressions

For electrochemical reaction at the cathode, the Butler–Volmer equation is applied in the model using two rate coefficients because the reactions (Eq. II) depends on both concentration of Li^+ and oxygen and concentration of Li_2O_2:

$$\frac{j_c}{nF} = k_a\left(c_{Li_2O_2,s}\right)exp\left[\frac{(1-\beta)nF}{RT}\eta_c\right] - k_c\left(c_{Li^+,s}\right)^2\left(c_{O_2,s}\right)exp\left[\frac{-\beta nF}{RT}\eta_c\right] \quad (15)$$

$$\eta_c = \phi_1 - \phi_2 - \Delta\phi_{film} - E^0 \quad (16)$$

$$\Delta\phi_{film} = j_c R_{film}\varepsilon_s \quad (17)$$

where j_c is local transfer current density between electrode and electrolyte interface, $c_{i,s}$ is the molar concentration of species i at the wall or surface of electrode, k_a and k_c are the anodic and cathodic rate constant, respectively, β is the symmetry factor equal to 0.5, η_c is surface or activated overpotential for reaction at cathode, $\Delta\phi_{film}$ and R_{film} are the voltage drop and the electrical resistivity across Li_2O_2 film formation, respectively, ε_s is the volume fraction of solid Li_2O_2, and E^0 is the theoretical open-circuit potential for reaction.

Whereas the electrochemical reaction at the lithium metal anode, it is given by the general Butler–Volmer equation as follow

$$j_a = i_0\left[exp\left(\frac{(1-\beta)nF}{RT}\eta_a\right) - exp\left(\frac{-\beta nF}{RT}\eta_a\right)\right] \quad (18)$$

where i_0 is exchange current density for anode, η_a is surface or activated overpotential for reaction at anode, and the other parameter are as described above.

The specific area a of the electrode/electrolyte interface in Eq. (13) is decreased by the morphology and dynamic change of the porosity due to the Li_2O_2 solid passivation during electrochemical reaction. This effective local surface area per unit volume of electrode can be commonly written by a geometric relation [12,18]

$$a = a_o\left[1 - \left(\frac{\varepsilon_{Li_2O_2}}{\varepsilon^o}\right)^p\right] \quad (19)$$

where $\varepsilon_{Li_2O_2}$ and ε are the volume fraction of solid Li_2O_2 and initial electrode porosity, respectively. This empirical equation is used to describe the change in the interfacial area for electrochemical reactions that occur during discharge because of the fast passivation of Li_2O_2 covering a portion of the active sites for electrochemical reaction over the carbon surface [19]. The magnitude of exponent p is a geometrical factor indicating the morphology shape of the solid peroxide that covers the active area. Small values of p indicate that the flat, plate-like precipitate of Li_2O_2,

conversely, large values of p reflects the needle-like solid which cover small active area. In this model, the value of 0.5 has been used.

2.4. Transport through Li_2O_2 layer

During discharge at a short period of time, a thin Li_2O_2 layer could be formed continuously, covering the active carbon surface. Hence, the diffusion of Li^+ and O_2 reactants from the porous media has the additional transport resistance through the Li_2O_2 layer. In other word, the active reactants transport comprise of two types of diffusion regimes as shown in Fig. 2. The first one is diffusion of Li^+ and O_2 reactants along the porous media and the other is their pass through the Li_2O_2 layer. The latter transport can be derived according to Fick's law, which is proportional to concentration gradient between bulk and active surface, corresponding with the electrochemical reaction in which each species is consumed at the active electrode surface (Eq. (14)).

$$-\frac{as_i}{nF}j_c = \frac{aD_{i,film}(c_i - c_{i,s})}{l} \tag{20}$$

where $D_{i,film}$ is the effective diffusion coefficient of species i across the Li_2O_2 film, l is the thickness of the film which is calculated from the volume fraction of the solid discharge products given by Eq. (23). However, preliminary simulated calculation showed that the difference between c_i and $c_{i,s}$ is significant only when c_i is high. The porosity volume change of the carbon electrode will be decreased due to the formation of insoluble Li_2O_2 covering the catalyst and active particles as described in Eq (21). Thus, the effective diffusivity for both Li^+ and oxygen reactants is used to describe how the pores are deposited by the Li_2O_2 formation; this can be described by the Bruggeman relationship.

$$\frac{\partial \varepsilon}{\partial t} = aj_c\frac{M_{Li_2O_2}}{2F\rho_{Li_2O_2}} \tag{21}$$

The volume fraction of the solid Li_2O_2 formation can be determined from the cathode volume balance as

$$\varepsilon_{Li_2O_2} = 1 - \varepsilon - \varepsilon^o \tag{22}$$

$$l = \left(\frac{\varepsilon_{Li_2O_2} + \varepsilon_s^0}{\varepsilon_s^0}\right)^{1/3} r_0 - r_0 \tag{23}$$

where $M_{Li_2O_2}$ and $\rho_{Li_2O_2}$ are the molecular weight and the mass density of Li_2O_2, respectively, ε_s^0 is the volume fraction of initial solid phase of cathode electrode (active carbon, catalyst and binder), and r_0 refers to the particle radius in the electrode.

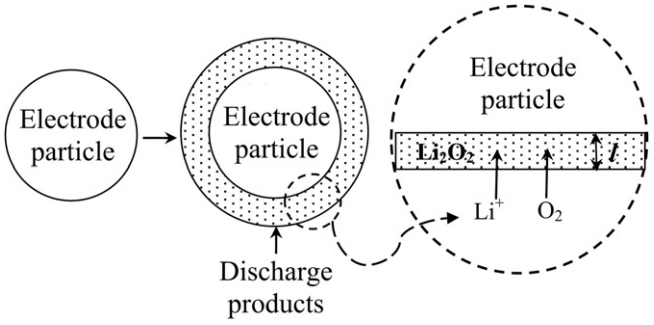

Fig. 2. Schematic diagram of reactants transport inside the porous electrode and the growth of discharge product on the surface of spherical electrode particle. The inset shows the enlargement of diffusion transport through the barrier of Li_2O_2 layer, l.

2.5. Assumptions

The following assumptions are used in this model:

- The Li_2O_2 is the main reaction product (Eq. II) and is only formed inside the porous cathode.
- The electrolytes used in Li–air batteries are assumed a binary monovalent electrolyte which consists of a single salt in a homogeneous organic solvent mixture.
- The Li^+ diffusion could be simulated by the concentrated solution theory. The pores within cathode are full of liquid phase electrolyte.
- The oxygen is assumed to dissolve in the organic electrolyte with the saturated concentration initially.
- The convection for mass transport is negligible inside the cell.
- The Li–air cell is operated in isothermal condition so that the thermal effect is not considered.

2.6. Initial conditions

At the start of the discharge process, initial conditions are specified for the Li^+ and oxygen concentrations, the porosity, the specific interfacial area, and the cell thickness. These initial values applied in the Li–air battery model are adopted from literature and summarised in Table 1. Before starting the discharge battery, the concentration for each species is assumed to be uniformly at all locations inside the cell system and equals to their initial concentration. Because the thickness of the porous cathode is much larger than both of APL and separator, then this area is regarded as the main part affecting the cell performance.

2.7. Boundary conditions

From Fig. 1, a schematic view of the model cell consists of four boundaries and three regions. The constant for oxygen concentration feeding at the right side of the cathode ($x = L$) can be estimated form the oxygen solubility (S_{O_2}) and the external concentration ($c_{O_2,ext}$)as shown in Table 1. At the current collector or the back side of the carbon electrode ($x = L$), the current density in the solid phase is equal to the applied discharge current density, the current density in the electrolyte phase equals to zero, and the flux of each species is zero. At the carbon electrode/separator interface ($x = L_c$) the continuous boundary conditions are specified for the fluxes of all species. The current density in the solid phase in this interface becomes zero, and the current density in the electrolyte then equals to the applied discharge current density. The voltage of the cell is calculated by the difference between the electrode potential at cathode current collector and the electrolyte potential at the anode side, $V_{cell} = \phi_1(x = L) - \phi_2(x = 0)$.

The conservation equations and the boundary conditions described above were discretized using a finite element method and solved in one-dimensional battery system by commercial software package COMSOL multiphysics version 4.2a. The COMSOL software is designed to solve a set of coupled differential and algebraic equations and the battery simulation model is performed on a 32 bit Windows platform with 4 GB RAM, and Intel Core 2 Duo 2.93 GHz processor. The different transport equations and the electrochemical reactions were solved as time dependent. The solution were considered as converged solution when the difference between two results was less than 10^{-4} (relative tolerance) for all variables.

Table 1
Parameters used in simulation.

Parameter	Value	Unit	Symbol	Ref.
Cell properties				
Thickness of APL	5×10^{-8}	m	L_A	[4]
Thickness of separator	5×10^{-5}	m	L_C	[4]
Thickness of porous positive electrode	7.5×10^{-4}	m	L	[4]
Conductivity of positive electrode	10	S m^{-1}	σ	[14]
Porosity	0.73	–	ε^o	[26]
Specific interfacial area of cathode	3.75×10^6	m^2 m^{-3}	a	Calculated
Electrical resistivity across Li_2O_2 film formation	50	Ω m^2	R_{film}	[35]
Electrolyte properties				
Electrolyte concentration	1000	mol m^{-3}	$c_{Li,0}$	[7]
Solubility factor of oxygen	0.38	–	S_{O_2}	[14]
External oxygen concentration in air at 1 atm	9.46	mol m^{-3}	$c_{O_2,ext}$	[14]
Initial oxygen concentration at $x = L$ ($S_{O_2} * c_{O_2,ext}$)	3.264	mol m^{-3}	$c_{O_2,0}$	[14]
Solubility limit of Li_2O_2 dissolved in electrolyte	0.09	mol m^{-3}	c_{max}	[36]
Li^+ diffusion coefficient[a]	2.11×10^{-9}	m^2 s^{-1}	D_{Li}	[33]
Oxygen diffusion coefficient	7×10^{-10}	m^2 s^{-1}	D_{O_2}	[10]
Conductivity of Li^+ in electrolyte	1.085	S m^{-1}	κ	[37]
Transference number of Li^+[a]	0.2594	–	t_+	[38]
$\partial lnf/(\partial lnc_{Li})$[a]	−1.03	–	–	[38]
Kinetic parameters				
Reaction rate coefficient anodic current	1.11×10^{-15}	m s^{-1}	k_a	Assumed
Reaction rate coefficient cathodic current	3.4×10^{-17}	m^7 s^{-1} mol^{-2}	k_c	Assumed
Dissolution rate coefficient of Li_2O_2	4.0	s^{-1}	k_d	Assumed
Exchange current density for anode	1	A m^{-2}	i_0	Assumed
Symmetry factor	0.5	–	β	[14]
General parameter				
Mass density of Lithium peroxide (Li_2O_2)	2140	kg m^{-3}	$\rho_{Li_2O_2}$	[39]
Mass density of electrolyte solution ($LiPF_6$)	1200	kg m^{-3}	ρ_{LiPF_6}	[39]
Mass density of carbon	2260	kg m^{-3}	ρ_c	[39]
Particle radius in the electrode	25×10^{-9}	m	r_0	[6]
Operating temperature	300	K	T	

[a] Vary with concentration.

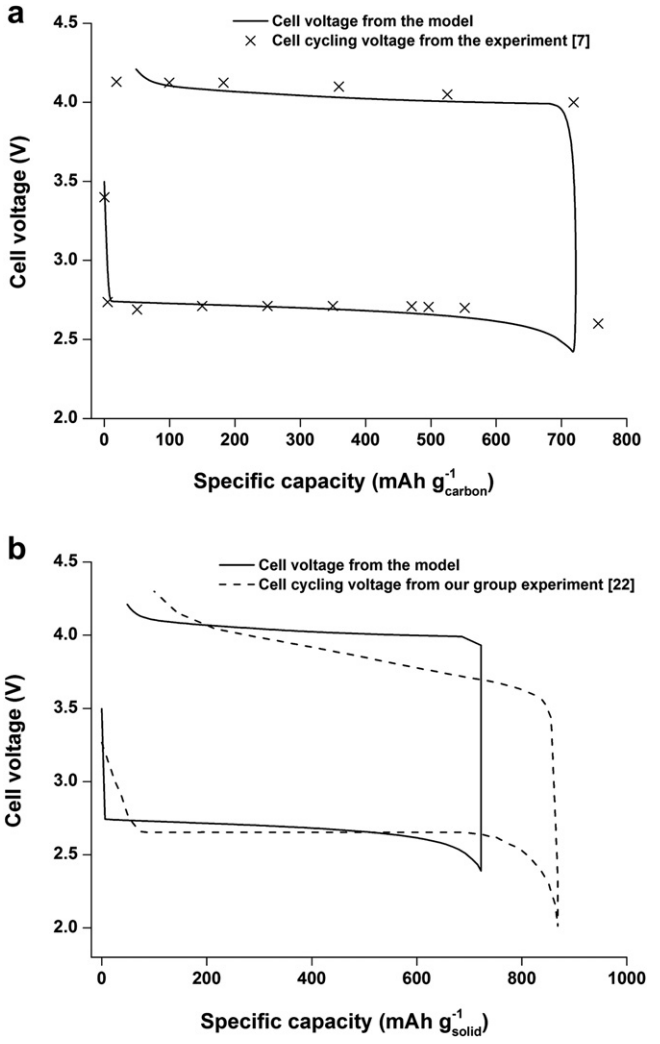

Fig. 3. Voltage–capacity curve on discharge then charge for a nonaqueous Li–air battery at a rate of 0.1 mA cm^{-2}. The electrolyte contains 1 M $LiPF_6$ dissolved in acetronitrile. The oxygen solubility factor in the electrolyte is 0.38. The cathode electrode thickness is 750 μm with porosity of 0.73. The cell cycle is simulated between 2.4 and 4.2 V in pure 1 atm of oxygen at operating temperature 300 K. (a) The model comparing to published data. (b) The model comparing to our group experiment.

3. Results and discussion

3.1. Effect of applied current density

The simulated voltage–capacity curve of the Li–air battery during discharge and then charge in 1 M $LiPF_6$ dissolved in an organic solvent between 2.4 and 4.2 V vs. Li/Li^+ at 0.1 mA cm^{-2} is shown in Fig. 3a. It can be seen from the figure that the simulated results match well to the experimental voltage during discharge at 1 atm of oxygen [7]. During discharge, the cell potential fell steeply at the beginning, from a voltage of 3.4 V to a plateau at around 2.7 V, and decreased continuously to 2.4 V. The discharge cell potential around 2.5–2.7 V was in good agreement with our group report previously for similar battery discharged in 1 atm oxygen as shown in Fig. 3b [20]. Although some of the parameters applied in the model are different from experimental data in Fig. 3b, the model results and experimental data showed similarities, suggesting that the model is a promising tool to identify the Li–air cell mechanisms and forecast the cell performance for design and scale-up. The discharge capacity for the case with the parameters in Table 1, based on the weight of carbon alone was about 802 mAh g^{-1}_{carbon}. As shown in Fig. 4, the discharge process was terminated by a rapid increase of polarisation at the end of discharge due to the oxygen concentration limitation resulting from solid Li_2O_2 formation on the cathode surface, inhibiting the flow of reactants (oxygen, Li^+, and electrons) to the active surface. Fig. 5a presents the oxygen concentration profiles inside the cell during battery discharging at various discharge states. The oxygen concentration decreases at the oxygen feed side of the cathode and oxygen cannot diffuse further inside the electrode because of the continuous growth of Li_2O_2 on the active surface of the porous carbon in an electrode diminishes the available pores for electrolyte resulting in either increasing Li_2O_2 insulated film or pore blocking. Both phenomena lead to restriction of oxygen transportation and severely limit the cell capacity. To overcome this problem, the suitable carbon material with a sufficiently large pore size distribution over the entire electrochemically active surface should be used as a cathode to provide enough space for the discharge products. The effect of different initial cathode porosities is presented later. The variation in porosity as a function of space and time for a discharge current of

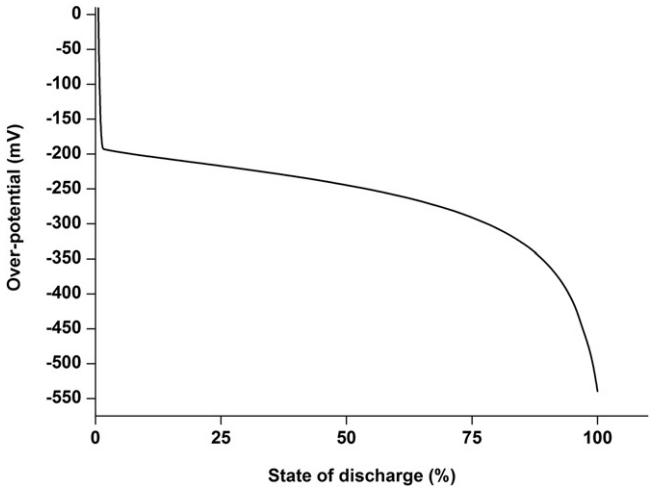

Fig. 4. Change of positive electrode over-potential during discharge at a rate 0.1 mA cm^{-2} at different discharge state (0% = battery is fully charged).

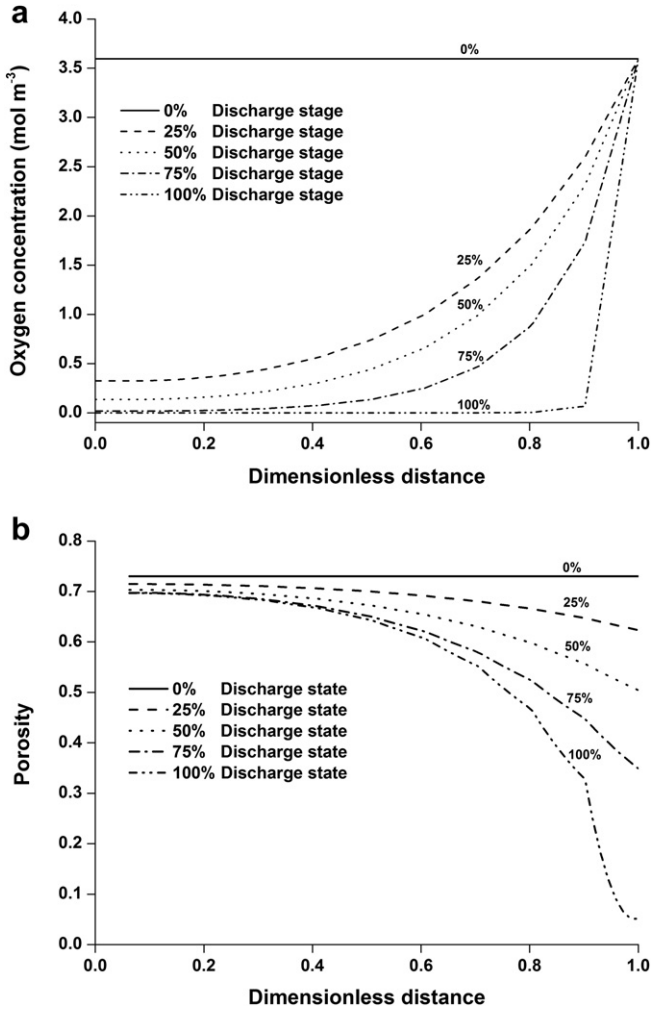

Fig. 5. Local (a) concentrations of oxygen and (b) porosity profile inside the Li–air cell during discharge at a rate 0.1 mA cm^{-2} at different discharge state (0% = battery is fully charged). The electrolyte contains 1 M $LiPF_6$ dissolved in acetronitrile. The oxygen solubility factor in the electrolyte is 0.38. The cathode electrode thickness is 750 μm with porosity of 0.73.

0.1 mA cm^{-2} is shown in Fig. 5b. As the diffusion coefficient of oxygen is very low compared to Li^+ species in this battery, the porosity falls predominantly at the oxygen feed side of the cathode. As the extent of discharge increases the porosity falls almost to zero and thus blocks the diffusion of oxygen species to into the cell.

Fig. 6 shows the effect of applied current density on the simulated discharge curves for a Li–air battery using the same cathode details as shown in Fig. 3. The discharge capacity demonstrates a large decrease from 1350 mAh g^{-1}_{carbon} at low current density 0.05 mA cm^{-2} to 213 mAh g^{-1}_{carbon} at a higher current density 1 mA cm^{-2}. This is consistent with experiments published by Read [7] and similar trend to the previous groups that the current density has significant effects on the cell capacity [21,22]. Moreover, the discharge voltage plateau is also lower with increasing current density. The capacity loss at high discharge rate can be discussed in term of transport limitation of oxygen diffusion through the cathode flooded with electrolyte which cannot maintain the electrochemical reaction. Thus, oxygen reduction occurs in a small region close to the cathode-current collector interface as the discharge rate increase. Moreover, the rapid porosity reduction due to the deposition of Li_2O_2 on the surface of the active area also limits oxygen transport into the cell and incompletely utilises the full capacity of the electrode porosity.

For battery on charge, then provided solid lithium peroxide ($\varepsilon_{Li_2O_2}$) has been produced there will be a finite Li_2O_2 concentration ($c_{Li_2O_2}$) dissolved in solution (saturation concentration) and the rate of oxidation reaction would be constant and will only decrease when the solid is consumed or $c_{Li_2O_2}$ goes below the solubility limit. Therefore, the model assumption applied on charge is that the dissolution rate (r_{diss}) of solid peroxide is fast compared to electrochemical reaction and can be written in Eq. (24). The dissolution rate equation is included for $c_{Li_2O_2}$ species balance in Eq. (1) during battery on charge and the driving force term for this reaction is when the $c_{Li_2O_2}$ decreases below its solubility in the electrolyte (c_{max}).

$$r_{diss} = k_d \varepsilon_{Li_2O_2} (c_{max} - c_{Li_2O_2}) \tag{24}$$

where k_d is the dissolution rate constant for Li_2O_2 during charge which assumed very fast, and c_{max} is the solubility limit of Li_2O_2 dissolved in organic electrolyte.

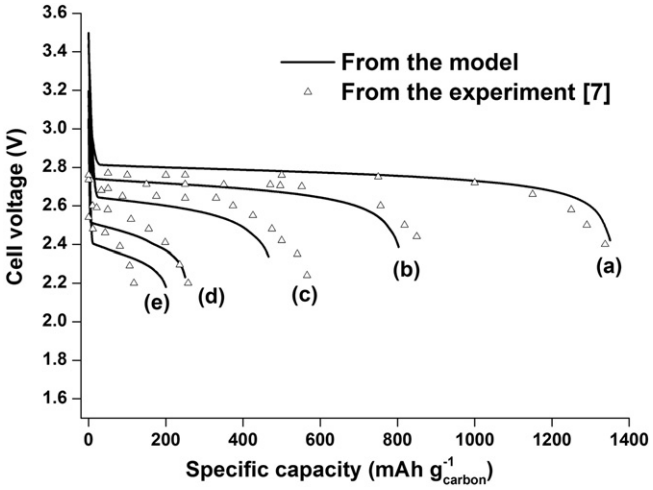

Fig. 6. Comparison of the voltage–capacity curve between the model and experiment for a nonaqueous Li–air battery at different discharge rate (a) 0.05 mA cm^{-2}, (b) 0.1 mA cm^{-2}, (c) 0.2 mA cm^{-2}, (d) 0.5 mA cm^{-2}, and (e) 1.0 mA cm^{-2}. The other parameters used in the model are the same as described in Fig. 3.

In the charge process, the voltage increased sharply to reach a plateau at about 4.0 V as shown in Fig. 3a and is consistent with the published charge curve at the same charging rate with a slightly difference [7]. The charge capacity is almost equal to its capacity when discharging. Hence, the model in which the published parameters are applied can be used to describe the Li–air battery behaviour as well as optimise the cell performance and will be compared later with the actual experimental data generated in our lab. Note that this model assumes Li_2O_2 as only discharge product and does not consider other possible parasitic reactions, although some side reactions, e.g. decomposition of organic solvent, could lead to undesired discharge products, such as Li_2CO_3, LiOH, and lithium alkyl carbonates [23–25].

3.2. Effect of oxygen solubility

One of the major drawbacks of current Li oxygen/air batteries is the low current densities at which the cell operates. The important factor that limits the performance of Li–air battery is the solubility of oxygen in the electrolyte. It is summarised from the work of Read et al. that to improve the performance of Li–air batteries, one should either increase the diffusion coefficient of oxygen or increase the oxygen solubility in the electrolyte to enhance the reaction rate of the cathode so that the solid Li_2O_2 efficiently fills in the pore [7,10]. In this section, the solubility of oxygen is varied in the model to simulate the cell cycling behaviour. In practical, this parameter can be increased by using solvent with high capability to dissolve oxygen, such as solvent based on perfluorinated solvents or ether-based electrolytes [26]. When the solubility of oxygen is increased from the base case of 3.6 mol m^{-3} to the higher solubility of oxygen concentration of 9.46 mol m^{-3}, the discharge specific capacity and specific energy of Li–air cell increase as shown in Fig. 7a. The battery capacity when discharged at a low current density 0.1 mA cm^{-2} increased from 802 mAh g_{carbon}^{-1} for the low oxygen solubility (oxygen concentration 3.6 mol m^{-3}) to 1400 mAh g_{carbon}^{-1} at the highest oxygen solubility (oxygen concentration 9.46 mol m^{-3}).

It is interesting to note that the difference in discharge capacity among the works reported previously [7,26–28] is largely a result of the diverse properties of electrolytes to dissolve the distinct amount of soluble oxygen. A recent study by Lu et al. [26] showed that the high discharge capacity of Li–air battery can be attributed to higher oxygen solubility in the electrolyte with 1,2-Dimethoxyethane (DME) used in his work comparing to lower capacity in the electrolyte with propylene carbonate (PC). From his work, the solubility of oxygen in the electrolyte with DME is around 8.76 mol m^{-3} providing the specific capacity 2600 mAh g_{carbon}^{-1} at low discharge current density of 250 mA g_{carbon}^{-1} (approximately 0.1 mA cm^{-2} in our simulation). This capacity is higher than our work with the same solubility of oxygen concentration. Many possible explanations could account for this but one factor might be that the diffusion coefficient for oxygen in our model (7×10^{-10} m^2 s^{-1}) is lower than the one in electrolyte with DME (4×10^{-9} m^2 s^{-1}) and the transference numbers describing the fraction of the total current carried by Li^+ in a solution are different between the two electrolytes. However, if these parameters are applied in our model including the solubility of oxygen in DME (8.76 mol m^{-3}) at low discharge current density of 0.1 mA cm^{-2}, the cell capacity from our simulation (2400 mAh g_{carbon}^{-1}) almost equals to the cell using DME electrolyte (the results is not shown here). Therefore, this model can be appropriately used to predict the behaviour of Li–air battery when changing detailed parameters.

Moreover, it can be seen from Fig. 7b that the discharge cell voltages also increased, from ca. 2.68 to 2.80 with the higher dissolved oxygen concentration in the electrolyte. The cell performance is enhanced because the oxygen can substantially diffuse farther inside the porous structure when a solvent with greater oxygen solubility is used. For the cell cycling, it is apparent from the same figure that no significant difference can be seen from the charge voltage of Li–air battery at various oxygen solubilities, i.e. increasing dissolved oxygen will not affect the cell performance significantly on the charging period as can be appreciated from the kinetic oxidation reaction.

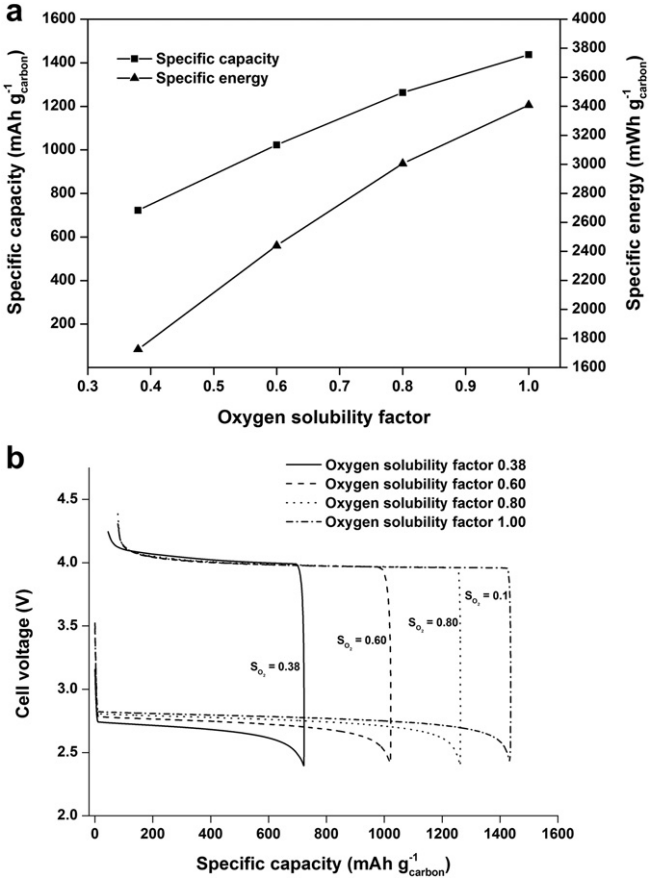

Fig. 7. Effect of oxygen solubility at a rate of 0.1 mA cm^{-2} on (a) specific capacity and energy and (b) voltage–capacity curve on discharge then charge for the Li–air battery. The other parameters used in the model are the same as described in Fig. 3.

3.3. Effect of lithium peroxide solubility

The discharge products of Li–air battery, Li_2O and Li_2O_2, are not very soluble in a non-aqueous electrolyte and also considered one of the main reasons that limit the cell performance. Therefore, introducing some additives or co-solvent to the cell electrolyte can partially enhance the solubility of the discharge products and improve the cell performance. It has been demonstrated that adding tris(pentafluorophenyl) borane (TPFPB) can substantially increase the solubility of Li_2O_2 in carbonate based solvent from very low amount of 0.19 mol m^{-3} to 190 mol m^{-3} [29]. Consequently, it is interesting to use the model to simulate the variation of Li_2O_2 solubility on performance. On addition of the TPFPB additive, not only is the lithium oxides solubility increased but also both the Li^+ transference numbers and the electrolyte conductivities are enhanced for those electrolytes with added TPFPB complex. These effects are not considered in our current model which is focused only the effect of Li_2O_2 solubility. From the data in Fig. 8a, it is apparent that increasing the solubility of Li_2O_2 in electrolyte does

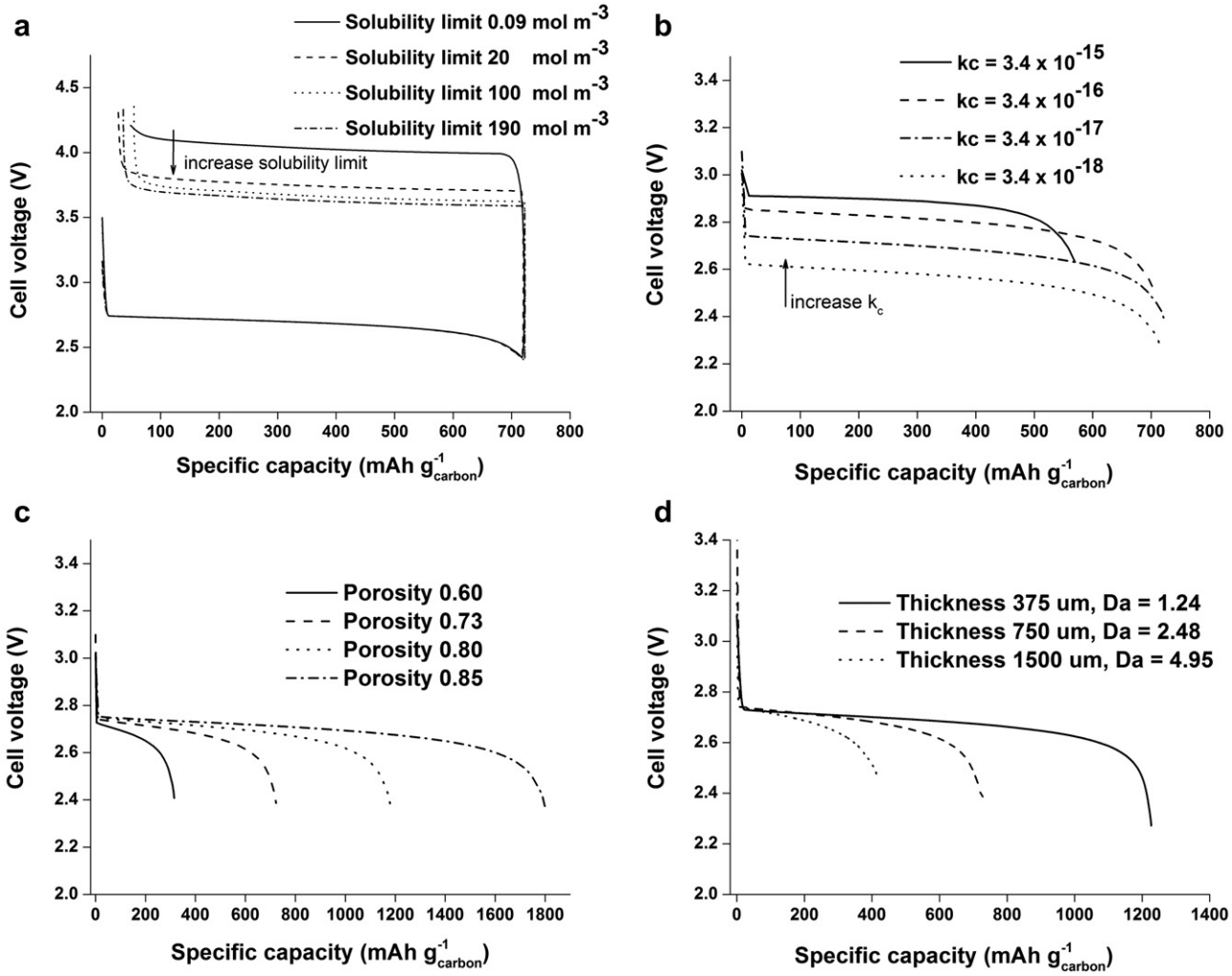

Fig. 8. Voltage–capacity curve on discharge then charge for the Li–air battery at a rate of 0.1 mA cm^{-2} as a function of (a) Li_2O_2 solubility factor and voltage–capacity curve on discharge as a function of (b) cathodic rate constant, (c) initial cathode porosity, and (d) cathode thickness. The other parameters used in the model are the same as described in Fig. 3.

not affect the discharge voltage and specific capacity of Li–air cell performance. However, there is a significantly improvement of the charge cycling cell voltage, i.e. the magnitude of charge voltage decreased by approximately 0.4 V with higher Li_2O_2 concentration dissolved in the electrolyte. The improvement on charge potential in the case of increasing the Li_2O_2 solubility is related to better surface oxidation reaction kinetics.

3.4. Effect of kinetic rate constant and porosity

As the cell performance depends on the porous electrode, one option is that the applied catalysts, such as metal oxide catalysts and noble metal catalysts, with carbon active materials can reduce the overpotential and thus increase the cell efficiency. To investigate the effect of different catalysts on the battery behaviour, the effect of cathodic rate constant (k_c) on the discharge voltage of the cell as a function of the specific capacity is shown in Fig. 8b. This rate coefficient is assumed constant and uniform distribution inside the cathode. As demonstrated in the results, the cell voltage plateau gradual increased with the higher value of k_c due to the reduced overpotential of the cathode electrode. The value of 3.4×10^{-16} of k_c demonstrated an onset voltage of about 2.85 V, and an average voltage plateau of 2.82 V (only 0.14 V lower than estimated equilibrium of 2.96 V for Li_2O_2 formation). This can be attributed to the reasonably high reduction reaction activity at the carbon/catalyst interface with higher catalyst activity. However, there was a relatively small increase in specific capacity of cathode with different rate constants. This study results do not support the previous researches [6,27,30] demonstrate that the various catalysts can improve both the specific capacity and discharge voltage. A possible explanation for this might be that the carbon porosity is modified by the reaction with catalyst during the preparation [31]. As a result, some of the closed micro-pores are opened for the greater access of discharge products, and some open pores are widened. However, this effect which influences the cell capacity was not included in our model with applying the same cathode structure (carbon loading, thickness and porosity).

For the case of varying initial cathode porosity, the results show that the battery capacity increases with the more space available to accommodate discharge products as presented in Fig. 8c. There is a slight increase in the voltage plateau for the higher porosity. Note that the battery capacity is normalised to the weight of carbon comprised in the cathode electrode. This value is also affected when the active material decreases in the cell using high porosity. Moreover, the porosity is assumed that there are no micro-pore

channels which is not utilised by lithium oxides inside the porous cathode.

3.5. Effect of cathode thickness

Besides concentrations and discharge conditions affecting the cell behaviour, the thickness of the cathode electrodes also plays an important role in the electrochemical performance. Fig. 8d shows the cell discharge voltage as a function of specific capacity for the different cathode thickness. Obviously, the thicker electrode provides the lower cell performance in term of specific capacity. This can be attributed to both the slow diffusion of oxygen dissolved in non-aqueous electrolyte and the long residence time moving through the thicker electrode. A number of experimental published works showed that the scanning electron microscopy (SEM) images of the cathode surface on the airside of the fully discharged cell were almost filled in the space by solid lithium oxides deposition [9,26,32], but this behaviour did not appear on the separator side. To investigate the effect of cathode thickness, the Damköhler number is introduced as shown in the equation below.

$$Da = \frac{j/nF}{D_{O_2,eff} \cdot c_{O_2}/L} \tag{25}$$

The Damköhler number defined in Eq. (25) expresses a dimensionless ratio of current density of electrochemical reaction rate to oxygen diffusion rate or this can be said that the ratio of the characteristic time of oxygen diffusion to the reaction time. A unity of Damköhler number means equal rate of surface electrochemical reaction and oxygen mass transport due to diffusion. From the Damköhler number for each cathode thickness in Fig. 8d, it is indicated that all the numbers are greater than unity and the higher value provides lower specific cell capacity when discharging Li–air at the current density of 0.1 mA cm^{-2}. When Damköhler number is large (more than unity), the Li–air performance is controlled by the diffusion of oxygen which has a low diffusion coefficient in non-aqueous electrolyte and also be affected by the tortuosity of porous cathode. As a result, the cell demonstrated the small specific capacity as the thicker electrode and high value for the thinner electrode. To further calculate the Damköhler number, Table 2 compares this number in different cell thickness and discharge current densities. The Damköhler number for the cathode thickness of 750 μm in different discharge rate as shown in Table 2 corresponds to the voltage–capacity curve in Fig. 6 which describes the better Li–air performance as the low Damköhler number at small discharge rate. This study has shown that, to meet the high cell performance, the cathode electrode should be an average in thickness around 500–750 μm and operates on the low current density. For the higher discharge rate or thicker cathode, the cell will be suffered from the diffusion-controlled limitation which can be overcome this problem by using the electrolyte with high solubility and diffusivity of oxygen to decrease the Damköhler number.

3.6. Electrolyte with high solubility Li_2O_2 additive

One of the main issues during the operation of Li–air cell is build up of the solid lithium peroxide depositing and covering the active surface of the porous cathode. From the previous section, some amount of boron complexes additive, e.g. tris(pentafluorophenyl) borane (TPFPB), can substantially increase the solubility of Li_2O_2 in carbonate based solvent within a limited concentration. Hence, it would be interesting to model the cell in the absence of solid oxide formation in case the electrolytes have high solubility of Li_2O_2.

Table 2
Comparison of Damköhler number in different cell thickness and discharge current densities for oxygen diffusion coefficient ($D_{O_2} = 7 \times 10^{-10} m^2 s^{-1}$).

Thickness (μm)	0.05 (mA cm^{-2})	0.1 (mA cm^{-2})	0.2 (mA cm^{-2})	0.5 (mA cm^{-2})
250	0.41	0.83	1.65	4.13
375	0.62	1.24	2.48	6.19
500	0.83	1.65	3.30	8.25
750	1.24	2.48	4.95	12.38
1000	1.65	3.30	6.60	16.51
1250	2.06	4.13	8.25	20.64
1500	2.48	4.95	9.91	24.76

Without solid formation, the porosity and active surface area inside the cathode are assumed constant during discharge operation. Then, the local concentration of Li_2O_2 increases continuously with time in the electrolyte. This may affect the density and viscosity of the electrolyte solution and the diffusivity of oxygen when high concentrations Li_2O_2 are encountered. The data for density of electrolyte depending on concentration of Li_2O_2 are not known, therefore, we have adopted the information of solution density dependent on $LiPF_6$ concentrations from [33]. The variation of electrolyte density is increased linearly with $LiPF_6$ concentration and the data is extrapolated to the desired concentration in the

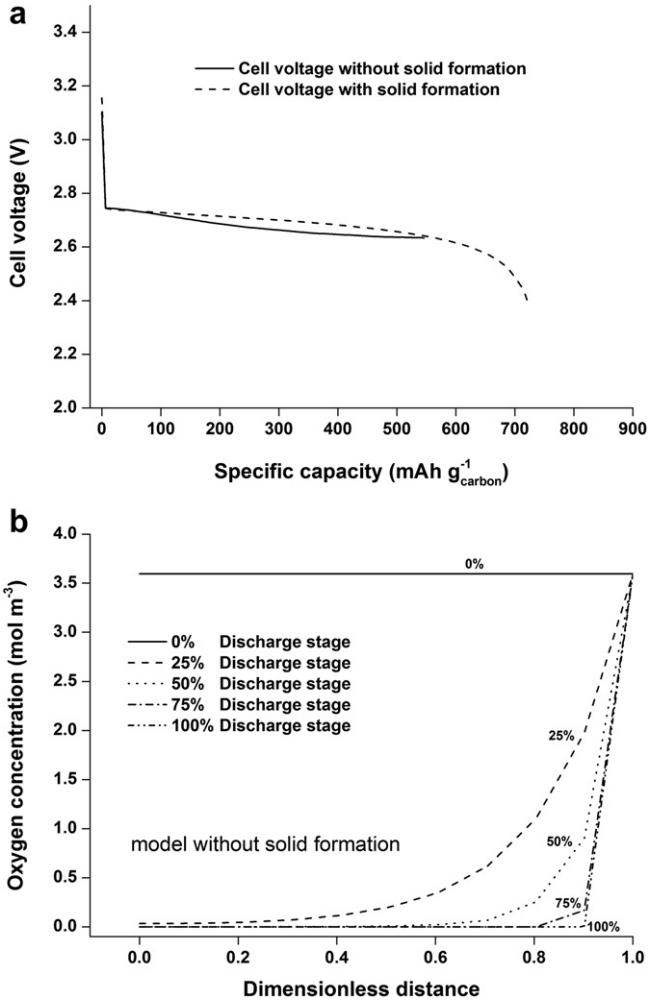

Fig. 9. (a) Comparison of the Li–air cell discharge voltage at a rate 0.1 mA cm^{-2} between cell with and without solid Li_2O_2 formation. (b) Local concentrations of oxygen profile inside the Li–air cell without solid Li_2O_2 formation during discharge at a rate 0.1 mA cm^{-2} at different discharge state (0% = battery is fully charged).

model. The volume of the cell system is assumed constant during simulation. Similarly, the solution viscosity also changes with salt concentrations and this relation is applied in the model. Changes et al. [34], had investigated the relative viscosity of concentrated electrolyte solution by applying the Jones–Dole equation which is used to describe the viscosity of solutions when the salt concentration is varied. Moreover, the diffusivity coefficient of oxygen decreases with increasing viscosity in the electrolyte. To describe this behaviour, the relationship between viscosity and the diffusion coefficient of oxygen is given by the Stokes–Einstein equation. The results of cell voltage discharge at 0.1 mA cm^{-2} obtained in both the model with and without of the solid lithium oxide formations are shown in Fig. 9a. The specific capacity predicted by the model without the formation of solid is almost equal to that from the model that includes the effect of the porosity change due to the solid formation. However, the former demonstrates slightly lower cell voltage compared to the latter. This effect may be from the result of the high density of electrolyte solution when highly soluble salts are encountered.

As the concentration of solution increased with time by assuming the high-dissolved discharge product of Li_2O_2, the oxygen diffusion rate fell because of the high salt concentration and increasing solution viscosity. It can be seen from the oxygen transport inside the porous cathode in Fig. 9b that the decrease in oxygen concentration with discharge time is greater than the case with Li_2O_2 formation (Fig. 5a) and the diffusion is limited close to the cathode/current collector interface owing to the high resistance of oxygen transport in a highly viscous solution.

4. Conclusions

A micro–macro homogeneous one-dimensional model has been developed for the rechargeable Li–air battery using a concentrated binary electrolyte theory. The model successfully predict the effects of applied current density, solubility limits for both oxygen and Li_2O_2, high degree of Li_2O_2 accumulation and the influence of the cathode structure. This model considers the time dependence and space dependence of the battery system and also includes the mass transport along the depth of the cell and the local mass transfer between Li_2O_2 layers and active surface morphology changing with the Li_2O_2 growth. The simulated cell potential for discharging is around 2.5–2.7 V and charging at around 4 V, which agree well with the experimental data. The nominal discharge capacity based on weight of carbon alone at 0.1 mA cm^{-2} is about 802 mAh g^{-1}_{carbon}, which is in agreement with the experimental observation. Increasing the solubility limit of oxygen enhances the discharge capacity and also increases the cell discharge potential, but does not affect the charge potential. Improving the solubility of Li_2O_2 in the electrolyte can lower the charging voltage but has little effect on the cell capacity. The present model can predict the potential and capacity of the battery and correlated the battery performance to parameters of reaction species and cathode structures with a reasonable accuration.

Acknowledgements

The authors would like to thank the Ministry of Science and Technology, Royal Thai Government for funding Ukrit Sahapatsombut PhD research and to the UK EPSRC for funding under grant number EP/I022570/1.

Nomenclature

a	specific interfacial area (m^2 m^{-3})
c_i	concentration of species i (mol m^{-3})
$c_{i,s}$	concentration of species i at the electrode active surface (mol m^{-3})
c_{max}	solubility limit of Li_2O_2 dissolved in organic electrolyte (mol m^{-3})
Da	Damköhler number
D_i	diffusion coefficient of species i (m^2 s^{-1})
$D_{i,eff}$	effective diffusion coefficient of species i (m^2 s^{-1})
$D_{i,film}$	diffusion coefficient of species i across the Li_2O_2 film (m^2 s^{-1})
E	electrode potential of cathode at any state (V)
E^0	electrode potential of cathode at standard state (V)
f	activity coefficient of $LiPF_6$ salt
F	Faraday's constant (96,485.34 C mol^{-1})
i_1	current density in the electrode phase (A m^{-2})
i_2	current density in the electrolyte phase (A m^{-2})
I	applied current density (A m^{-2})
j	interfacial transfer current density (A m^{-2})
k	reaction rate constant
l	thickness of the Li_2O_2 film formation (m)
L_A,L_C,L	thickness of APL, separator, and porous cathode respectively (m)
m_i	mass of species i (kg)
M_i	symbol for the chemical formula or molecular weight of species i (mol kg^{-1})
n	number of electrons transferred in the electrode reaction
N_i	molar flux of species i (mol m^{-2} s^{-1})
p	surface effect factor
r	particle radius (m)
r_i	reaction rate term in Eq. (1) that accounts for electrochemical and chemical reactions (mol m^{-3} s^{-1})
R	universal gas constant (8.3143 J mol^{-1} K^{-1})
R_{film}	electrical resistivity across Li_2O_2 film formation (Ω m^2)
s_i	stoichiometric coefficient of species i in electrode reaction
S_{O_2}	solubility factor of O_2 in non-aqueous electrolyte
t	time (s)
t_+	transference number of cation in electrolyte
T	temperature (K)
V_{cell}	cell voltage (V)
z_i	valence of charge number of species i

Greek letters

β	symmetry factor
δ	dimensionless parameter for LI $\beta nF/RT$ $(1/\kappa + 1/\sigma)$
ε	porosity or void volume fraction of porous cathode
ε_s	volume fraction of initial solid phase of cathode electrode
$\varepsilon_{Li_2O_2}$	volume fraction of solid Li_2O_2 formation in porous cathode
η	surface or activated overpotential (V)
κ	conductivity of electrolyte (S m^{-1})
κ_{eff}	effective conductivity of electrolyte (S m^{-1})
ν	number of moles of ions into which a mole of electrolyte dissociates
ν_+	numbers of moles of cations produced by the dissociation of a mole of electrolyte
ρ_i	density of a solid phase of species i (kg m^{-3})
σ	conductivity of the electrode (S m^{-1})
σ_{eff}	effective conductivity of the electrode (S m^{-1})
ϕ_1	electric potential in the electrode (V)
ϕ_2	electric potential in the electrolyte (V)
$\Delta\phi_{film}$	voltage drop across Li_2O_2 film formation (V)
∇	differential operator

Subscripts and Superscripts

o	initial
1	electrode phase

2	electrolyte phase
a	anodic
c	cathodic
diss	dissolution

References

[1] K.M. Abraham, Z. Jiang, Journal of the Electrochemical Society 143 (1996) 1–5.
[2] T. Ogasawara, A. Débart, M. Holzapfel, P. Novák, P.G. Bruce, Journal of the American Chemical Society 128 (2006) 1390–1393.
[3] T. Kuboki, T. Okuyama, T. Ohsaki, N. Takami, Journal of Power Sources 146 (2005) 766–769.
[4] J.G. Zhang, D. Wang, W. Xu, J. Xiao, R.E. Williford, Journal of Power Sources 195 (2010) 4332–4337.
[5] C.O. Laoire, S. Mukerjee, K.M. Abraham, E.J. Plichta, M.A. Hendrickson, Journal of Physical Chemistry C 114 (2010) 9178–9186.
[6] H. Cheng, K. Scott, Journal of Power Sources 195 (2010) 1370–1374.
[7] J. Read, Journal of the Electrochemical Society 149 (2002) A1190–A1195.
[8] Z. Peng, S.A. Freunberger, L.J. Hardwick, Y. Chen, V. Giordani, F. Bardé, P. Novák, D. Graham, J.M. Tarascon, P.G. Bruce, Angewandte Chemie – International Edition 50 (2011) 6351–6355.
[9] S.S. Zhang, D. Foster, J. Read, Journal of Power Sources 195 (2010) 1235–1240.
[10] J. Read, K. Mutolo, M. Ervin, W. Behl, J. Wolfenstine, A. Driedger, D. Foster, Journal of the Electrochemical Society 150 (2003) A1351–A1356.
[11] J. Newman, W. Tiedemann, AIChE Journal 21 (1975) 25–41.
[12] C.Y. Wang, W.B. Gu, B.Y. Liaw, Journal of the Electrochemical Society 145 (1998) 3407–3417.
[13] S. Sandhu, J. Fellner, G. Brutchen, Journal of Power Sources 164 (2007) 365–371.
[14] P. Andrei, J.P. Zheng, M. Hendrickson, E.J. Plichta, Journal of the Electrochemical Society 157 (2010).
[15] J. Newman, K.E. Thomas-Alyea, Electrochemical Systems, third ed., John Wiley & Sons, New York, 2004.
[16] W.A.v. Schalkwijk, B. Scrosati, Advances in Lithium-ion Batteries, Kluwer Academic/Plenum Publishers, New York, 2002.
[17] D.A.G. Bruggeman, Annalen der Physik (Leipzig) 24 (1935) 636–679.
[18] R.M. LaFollette, D.N. Bennion, Journal of the Electrochemical Society 137 (1990) 3701–3707.
[19] X. Ren, S.S. Zhang, D.T. Tran, J. Read, Journal of Materials Chemistry 21 (2011) 10118–10125.
[20] H. Cheng, K. Scott, Applied Catalysis B: Environmental 108-109 (2011) 140–151.
[21] J. Xiao, D. Wang, W. Xu, R.E. Williford, J. Liu, J.G. Zhang, Journal of the Electrochemical Society 157 (2010) A487–A492.
[22] S.S. Zhang, K. Xu, J. Read, Journal of Power Sources 196 (2011) 3906–3910.
[23] S.A. Freunberger, Y. Chen, N.E. Drewett, L.J. Hardwick, F. Bardé, P.G. Bruce, Angewandte Chemie – International Edition 50 (2011) 8609–8613.
[24] S.A. Freunberger, Y. Chen, Z. Peng, J.M. Griffin, L.J. Hardwick, F. Bardé, P. Novák, P.G. Bruce, Journal of the American Chemical Society 133 (2011) 8040–8047.
[25] B.D. McCloskey, D.S. Bethune, R.M. Shelby, G. Girishkumar, A.C. Luntz, Journal of Physical Chemistry Letters 2 (2011) 1161–1166.
[26] Y.-C. Lu, D.G. Kwabi, K.P.C. Yao, J.R. Harding, J. Zhou, L. Zuin, Y. Shao-Horn, Energy & Environmental Science 4 (2011) 2999–3007.
[27] A. Debart, J. Bao, G. Armstrong, P.G. Bruce, Journal of Power Sources 174 (2007) 1177–1182.
[28] A. Debart, A.J. Paterson, J. Bao, P.G. Bruce, Angewandte Chemie – International Edition 47 (2008) 4521–4524.
[29] B. Xie, H.S. Lee, H. Li, X.Q. Yang, J. McBreen, L.Q. Chen, Electrochemistry Communications 10 (2008) 1195–1197.
[30] Y.C. Lu, H.A. Gasteiger, M.C. Parent, V. Chiloyan, Y. Shao-Horn, Electrochemical and Solid-State Letters 13 (2010) A69–A72.
[31] N. Ominde, N. Bartlett, X.Q. Yang, D. Qu, Journal of Power Sources 185 (2008) 747–753.
[32] X.H. Yang, Y.Y. Xia, Journal of Solid State Electrochemistry 14 (2010) 109–114.
[33] S.G. Stewart, J. Newman, Journal of the Electrochemical Society 155 (2008) F13–F16.
[34] A. Chagnes, B. Carré, P. Willmann, D. Lemordant, Journal of Power Sources 109 (2002) 203–213.
[35] Q. Li, H.Y. Sun, Y. Takeda, N. Imanishi, J. Yang, O. Yamamoto, Journal of Power Sources 94 (2001) 201–205.
[36] K. Tasaki, A. Goldberg, J.J. Lian, M. Walker, A. Timmons, S.J. Harris, Journal of the Electrochemical Society 156 (2009) A1019–A1027.
[37] C.M. O'Laoire, in: Chemistry and Chemical Biology, Northeastern Universiy, Boston, Massachusetts, 2010.
[38] A. Nyman, M. Behm, G. Lindbergh, Electrochimica Acta 53 (2008) 6356–6365.
[39] D.R. Lide, CRC Handbook of Chemistry and Physics, 87th ed., Taylor & Francis, Boca Raton, Florida, 2007.